Mitochondria form cholesterol tethered contact sites with the Nucleus to regulate retrograde response

Radha Desai[1, 10*], Daniel A East[1*], Liana Hardy[1], James Crosby[1], Manuel Rigon[1], Danilo Faccenda[1], María Soledad Alvarez[1], Arti Singh[1], Marta Mainenti[1], Laura Kuhlman Hussey[1], Robert Bentham[2], Gyorgy Szabadkai[2,3,4], Valentina Zappulli[5], Gurtej Dhoot[1], Lisa E Romano[8], Xia Dong[1], Anne Hamechar-Brady[9], J Paul Chapple[8], Roland A. Fleck[6], Gema Vizcay-Barrena[6], Kenneth Smith[1] and Michelangelo Campanella[1,2]

[1]Department of Comparative Biomedical Sciences, The Royal Veterinary College, University of London, Royal College Street NW1 0TU, London, United Kingdom; [2]Department of Cell and Developmental Biology, Consortium for Mitochondrial Research (CfMR), University College London, Gower Street, WC1E 6BT, London, UK; [3]Department of Biomedical Science, University of Padua, Via Ugo Bassi, 35131, Padua, Italy; [4]Francis Crick Institute, Midland Road, NW1 AT, London, UK; [5]Department of Comparative Biomedicine and Food Sciences, University of Padua, Viale G. Colombo, 35121 Padua, Italy; [6]Centre for Ultrastructural Imaging, King's College London, London SE1 1UL, UK; [7]Pathobiology and Population Sciences, The Royal Veterinary College, Hawkshead Lane, North Mymms, Hatfield, Hertfordshire, AL9 7TA UK; [8]William Harvey Research Institute, Barts and the London School of Medicine, Queen Mary University of London, London EC1M 6BQ, United Kingdom [9]W. Harry Feinstone Department of Molecular Microbiology & Immunology, Johns Hopkins University Baltimore, MD 21205 USA. [10]Current address: Discovery Research MRL UK, MSD, The London Bioscience Innovation Centre (LBIC),2 Royal College Street, London, NW1 0NH

*The authors wish to acknowledge RD and DE as equal contributors

To whom correspondence should be addressed:

Michelangelo Campanella

Email: mcampanella@rvc.ac.uk

Royal College Street, London, NW1 0TU, UK

Abstract

Cholesterol metabolism is pivotal to cellular homeostasis, hormone production, and membrane composition. Its dysregulation is associated with malignant reprogramming and therapy resistance in neoplastic progression. Cholesterol is trafficked into the mitochondria for steroidogenesis by the transduceome protein complex, which assembles on the outer mitochondrial membrane (OMM). The highly conserved, cholesterol-binding, stress-reactive, 18kDa translocator protein (TSPO) is a key component of this complex. Here, we modulate TSPO to study the process of mitochondrial retrograde signalling with the nucleus, by dissecting the role played by cholesterol and its oxidized forms. Using confocal and ultrastructural imaging, we describe that TSPO enriched mitochondria, remodel around the nucleus, forming cholesterol-enriched domains (or contact sites). This dynamic is controlled by the molecular and pharmacological modulation of TSPO, which is required to establish the Nucleus-Associated Mitochondria (NAM) and hence implement pro-survival signalling in aggressive forms of breast cancer. This work provides the first evidence for a functional and biomechanical tethering between mitochondria and nucleus thus establishing a new paradigm in cross-organelle communication.

Key words: mitochondria, cholesterol, mitophagy, NF-kB and TSPO

Introduction

Mitochondria actively participate in remodelling and reprogramming of mammalian cells[1]. In response to stress, either of endogenous or exogenous nature, they retro-communicate with the nucleus to induce wide-ranging cytoprotective effects that sustain proliferation and surivival[2,3]. This Mitochondrial Retrograde Response (MRR), is exploited in the pathological context and primarily driven by deregulation of Reactive Oxygen Species (ROS), Ca^{2+} signalling and energy deficits which promote nuclear stabilization of transcription factors (e.g. nuclear factor kappa-light-chain-enhancer of activated B cells, NF-kB) to drive metabolic rewiring and resistance mechanisms[3-5]. In hormone-dependent tumours, such as those of the mammary gland, the therapeutic failure of endocrine therapy (ET) is linked with alterations in the cholesterol metabolism[6,7]. Cholesterol and cholesterol-derived intermediates are recognised determinants in the oncogenic reprogramming of hormone responsive cancer cells[6]. Metastatic, ET-resistant breast cancer cells show increased expression of CYP19A1, a member of the cytochrome C p450 monooxygenase enzymes[7], which catalyses the last steps of oestrogen synthesis from cholesterol. This prompted the question whether mitochondrial pathways associated with lipid transport are important players of this adaptive response, and whether a physical interaction is established to expedite this route of cellular communication. We sought to answer these fundamental questions by investigating the role played by the 18kDa mitochondrial protein TSPO[8], which translocates cholesterol from the outer into the inner mitochondrial environment. TSPO is overexpressed in cancer cells[4,9], therefore representing a logical target to determine the interplay between the lipid and the MRR[2,4] in pathophysiology.

The features driving retrograde (mitochondria to nucleus) communication[10] are a consequence of mitochondrial dysfunction[11-14], this is well reflected by the marked upregulation of TSPO resulting in intracellular redox-stress (ii), impaired cytosolic Ca^{2+} transients (iii), and cholesterol accumulation (iii). TSPO is localised on the Outer

Mitochondrial Membrane (OMM) and is detected at higher levels in aggressive mammary lesions[15-17]; besides taking part in the synthesis the steroids[18-20], it impairs the quality control of the organelle via autophagy (mitophagy)[21,22] and alters intracellular signalling pathways [22,23]. TSPO has previously been shown to have anti-apoptotic activity[24] and its ligands have consequently been tested as chemotherapy co-adjuvants[25] as well as PET-biomarkers of metastases[26,27]. Additionally, we know that inhibition of cholesterol synthesis improves mitochondria driven apoptosis[28], in spite of this, the role of TSPO and mitochondria in the management of intracellular cholesterol in a pathophysiological context remains relatively unexplored. We therefore tested whether in response to pro-apoptotic stressors, accumulation of TSPO and cholesterol on OMM primes the expression of pro-survival genes[29] and whether this is instrumental for efficient mitochondrial retro-communication with the nucleus.

Using cellular and ultrastructural imaging along with protocols for cholesterol dynamics, we have detailed an axis of cross-organelle communication which operates via cholesterol hot-spots. Most notably, we discovered that during this process, mitochondria become physically linked with the nucleus establishing contact sites for which TSPO is required. This interaction is indeed biochemically and pharmacologically controlled by targeting of the protein, implying that mito-nuclear contact sites represent both a biomarker of therapy resistance as well as a regulatory element in cellular rewiring to promote pathological evolution and uncontrolled proliferation.

Results

The first step of our analysis consisted in assessing the correlation between mitochondrial cholesterol handling and pro-survival transcriptional factors such as the NF-kB[30]. We therefore inspected primary human samples of mammary gland tumours for their pattern of TSPO and NF-kB expression reporting a positive association between TSPO level, aggressiveness of the lesions (**Figure 1 a, b**), and NF-κB[29,30] accumulation into the nucleus (**Figure 1d, e**). In line with this, transcriptomic analysis of >600 samples of breast cancer patients in the Cancer Genome Atlas (TCGA) showed higher levels of active NF-κB correlating with increased TSPO expression in the more aggressive types of tumours (HER positive and basal types) (**Figure 1c, f**), without detection of any mutation in TSPO (**SFigure 1a**). The increased expression of TSPO as underlying feature in the neoplasia of the mammary gland is notably retained across species implying a conserved mechanism of cellular adaptation to malignancy between human, dog and feline patients (**SFigure 1d-g**).

In order to elucidate the nature of this oncogenic interplay we moved the analysis into cell lines of human breast cancer and interrogated the biochemical mechanisms responsible for the cross-talk between TSPO expression and NF-κB nuclear translocation. We compared epithelial human breast cancer MCF-7 cells, which feature low TSPO levels, and the more aggressive counterpart MDA-MB-231 cells (henceforth referred to as MDA) derived from breast cancer adenocarcinoma which instead express high levels of TSPO[8] (**Figure 1g-h**). In MDA cells, TSPO was transiently knocked down (-TSPO) (**SFigure 1b**) before being exposed to Staurosporine (STS), used here as a mitochondrial stressor to engage the mitochondrial retrograde response. STS, which also stabilised TSPO presence (**SFigure 1c**), lead to concomitant nuclear translocation of NF-κB, which was biochemically mapped via means of cellular sub-fractionation thus corroborating the requirement for TSPO in the efficient repositioning of the transcription factor (**Figure 1j-l**). The outcome of the increased NF-kB retro-translocation was corroborated by the transcriptional profile of its regulated pro-

survival genes Bcl-2 and c-FLIP (**Figure 1n, o**) and protein expression of Bcl-2 (**Figure 1 q**). Immunocytochemical analysis further highlighted the degree of nuclear residency of the NF-κB upon STS treatment in MDA cells and how pruning of the mitochondrial network via pharmacological activation of mitophagy by the agent PMI[31,32] reduced the degree of NF-κB translocation in the same cells (**Figure 1n, o**). PMI by reducing the size of the mitochondrial network limits the mitochondrial space occupancy (**SFigure 1j**) sensitizes both human, feline and canine breast cancer cells to STS-induced apoptosis (**SFigure 2k-m**). Integrity of the mitochondrial network emerges therefore as pivotal to stabilise the retro-translocation and transcriptomic capacity of NF-κB induced by STS. Events which are on the other hand limited both the activation of mitophagy as well as treatment with the TSPO ligand PK11195 which competes with the cholesterol binding domains of the protein[33] (**Figure 2a, b**). Notably, the cholesterol synthesis inhibitor, pravastatin (PVS), succeeded in reducing the NF-κB translocation too thus implying that the TSPO-cargo cholesterol might facilitate the MRR **(Figure 2c).** Confirmation of the regulatory hierarchy between TSPO, cholesterol and NF-κB was provided by enrolling MDA cells constitutively knocked-out for NF-κB (NF-kB KO)[34] in which the additive affect exercised by the concomitant repression of TSPO was rather limited (**Figure 2d**). Knocking down of TSPO in MDA cells (-TSPO), in response to the pro-apoptotic cue STS, was in any case able to: increase sensitivity to apoptosis cross species (i) (**Figure 2e, SFigure 1 h, i**), reduce cellular proliferative capacity (ii) (**Figure 2f**), facilitate the accumulation of the pro-apoptotic molecule BAX on mitochondria (iii) (**Figure 2 g, h**) as well as to promote the release of cytochrome C release into the cytosol (iv) (**Figure 2i, j**). In keeping with this, TSPO ligands (**Table 1**) tangibly promoted chemically induced cell death, thereby co-adjuvating the effect of STS (**Figure 2 K**), as well as that of Doxorubicin or Vincristine (**Figure 2l, m**) both in bi-dimensional and in tri-dimensional ways of cells culturing (**SFigures 3c)**.

MCF-7 cells, which constitutively express lower levels of TSPO, gained resistance to STS-induced apoptosis, when the expression of the protein was forced but solely with the recombinant wild-type isoform whereas the mutant one lacking the Cholesterol Binding Domain CRAC (TSPOΔCRAC) failed to deliver such a protection (**Figure 3a-c**). This evidence implied that the cholesterol-binding capacity of TSPO is indeed crucial, as hinted by the data with its ligand PK11195, to ensure protection against cell death. And thus, in MCF-7 cells which have developed resistance to Tamoxifen (MCF7T[6]) or sparked their cholesterol bio-synthesis by long-term oestrogen deprivation (MCF7-LTED[6,35,36]) the expression level of TSPO is indeed greater (**Figure 3d, e**).

This made us investigate whether treatment with the TSPO ligand FGIN-127, equally capable as PK11195 to impair handling of cholesterol by the protein, could operate as deterrent against the nuclear accumulation of the Estrogen Receptor alpha (ERα). The nuclear internalization of the ERα is indeed a key event in the transition of epithelial breast tumour towards a more aggressive phenotype leading to therapeutic failure by first line of treatment such as with Tamoxifene[35,36]. FGIN-127 was beneficial in reducing the ERα association with the nucleus (**Figure 3 f, g)** as well as in increasing the degree of STS induced cell death in the same sub-set of cells (**Figure 3h**). The co-treatment was actually more beneficial in MCF7T than in standard MCF-7, likely due to the greater availability of targets (TSPO) in this cohort of cells. Aligning with these observations, big-data analysis revealed that TSPO is over-expressed in cohorts of relapsed breast cancer patients in whom Endocrine Therapy (ET) was no longer effective and cholesterol metabolism escalated (**Supplementary Figure 3a**).

Ultrastructure imaging analysis of MCF-7 cells via transmission electron micrography (TEM) also reported disrupted cristae and reduced mitochondrial-nuclear distance (passing from ~120nm to almost ~50nm in response to STS) (**Figure 3 i, j**) which prompted us to

investigate these inter-organelles association further and the mechanisms driving this relevant gain in space during induction of apoptosis.

Following co-immunocytochemical labelling of mitochondria with TSPO and nuclear envelope with the protein Lamin-B in both MCF-7 and MDA cells, we recorded that in the latter, and not in the former, mitochondria are constitutively present in the perinuclear region forming an association with the nucleus which is mirrored by infiltrates of TSPO positive mitochondria (**Figure 4a, b**). This phenomenon increased in response to STS as detailed both by immunoblotting of subcellular fractions (**Figure 4c, d**) and TEM analyses (**SFigure 2a, b**). TSPO, in response to STS, was indeed observed to be present in the portion of the cytosol occupied by mitochondria as well as in the nuclear envelope and in its core (**Figure 4c, d**). A dynamic redistribution which was promoted also by the mito-toxin Rotenone (ROT) which is well accounted as an MRR inducer (**Figure 4c, d**).

The ultrastructural imaging also revealed the prominent inter-organellar coupling which establishes the Nucleus-Associated Mitochondria (NAM) in MDA cells generating all-encompassing structure in and around the nucleus. Means of quantification revealed the formation of actual contact sites with a statistical reduction of distance-space between mitochondria and nucleus below 30nm and observable membrane fusion in some instances (**Figure 4e, f**).

The observed mitochondrial remodelling could therefore crucially influence the signalling of diffusible molecules such as ROS, which are acknowledged executors of the retrograde response[36]; ROS which indeed increase when TSPO is overexpressed (**Figure 4g-l**). The NAM induced change in space-distance would therefore favour the diffusion capacity of ROS maximizing their impact in the perinuclear and nuclear region. Notably, the remodelling of mitochondria on the nucleus, alike the retro-translocation of NF-kB, was limited by the mitophagy-driven trimming of the network during co-treatment with PMI[31](**Figure 4j-l**).

Formation of NAM is not specific of cancer cells though as we corroborated their existence also in Mouse Embryonic Fibroblasts (MEFs) in which the expression level of TSPO acts as a discriminant for these mito-nuclear contacts (**Figure 5a-f**). 'Variance' filter applied to confocal airy-scan images with immunofluorescence (LaminB1-ATPB) convincingly detail how the downregulation of TSPO (-TSPO) releases mitochondria from the nucleus whilst its overexpression (+TSPO) results in the coalescing of the mitochondrial network with the nuclear envelope (**Figure 5a-d**). These observations were corroborated at ultrastructural level via TEM analysis, which unequivocally showed the formation of contacts between mitochondria and nucleus in the face of increased TSPO expression (**Figure 5 e, f**). TSPO overexpressing MEFs also gained significant resistance to STS induced cell death, which was otherwise lost when the ΔTSPO-CRAC mutant isoform of the protein (unable to bind cholesterol) was expressed (**Figure 5 g**).

We then attempted to dissect the mechanisms by which TSPO could mediate such a tethering role between mitochondria and nucleus. We bio-informatically outlined TSPO interactors (**Figure 5h**) and among these teased out those with established anchoring capacity such as the ACBD3. The latter is recruited to mitochondria in a TSPO-dependent fashion[38]. The transient knocking down of ACBD3 in MDA cells (-ACBD3) succeeded in reducing the NAM at resting conditions but not during STS treatment, in which, its reduced expression just marginally prevented the frequency of contacts between mitochondria and nucleus**,** and TSPO-positive mitochondria still successfully invaded the nuclear space (**Figure 5i, j)**. Subsequently, we moved away from the known interactors of TSPO and tested whether the ER integral membrane protein VAPB5, which facilitates mitochondria-ER tethering, could be involved in the mechanism of organelles association. However, knocking down of VAPB5 in MDA cells (-VAPB5) did not modify the extent of NAM thus advocating for a tethering mechanism utterly distinct from the molecular repertoire involved in the ER-MAMs (**Figure 5 k-l, SFigure 3 j,m).**

All these data suggest that the TSPO mediated reduction of distance between mitochondria and nucleus could establish a relay between its cargo cholesterol and the increased ROS which do occur when TSPO is overexpressed. Auto-oxidation of cholesterol which results in oxysterol could therefore have in TSPO a key contributor and/or an amplifying link which would aid the etiopathology of several conditions including those characterized by malignant proliferation[38,39].

The exposure of MDA cells to 7-ketocholesterol (7-KC) (which is the second most abundant oxysterol found in mammals) does increase TSPO expression (**Figure 6 a-c**) and re-enforces the NAM (**Figure 6 d, e**). In response to 7-KC, a pattern of expression identical to the one of TSPO was mirrored by components of the steroidogenic protein complex-transduceome[19] ATAD3 and StAR as well as by LXR-β (**SFigure 2f-j**). Subsequently, in MDA cells expressing mito-RFP, co-labelled for Lamin-B1 we imaged cholesterol pools via the cholesterol-binding fluorescent compound, Filipin, which depicted the localization of cholesterol into foci close to and around the nucleus following STS treatment; foci which disappeared in -TSPO MDA cells (**Figure 6f, g**). The STS-induced re-distribution of cholesterol into in the nuclear envelope was then confirmed by the disordered membrane dynamics in result of accumulation of the lipid, imaged via the Di-4-ANEPPDHQ probe (**Figure 6h, i**). Additionally, the efflux of cholesterol from the nucleus could be observed during cell treatment with TSPO ligands (**Figure 6j**), as well its influx when the protein was overexpressed (**Figure 6 k**). Cholesterol trafficking was assessed live using a naturally fluorescent cholesterol analogue, dehydroergosterol (Ergosta)[40]. By measuring the Ergosta signal co-localized with mitochondria (demarked by Mitotracker Red) we reported that PK11195 prevents the invasion of the nuclear region by cholesterol (**Figure 6l, m)** as well as the perinuclear remodelling of the mitochondrial network during STS treatment (**Figure 6n, o**).

The inter-dependence between cholesterol accumulation in the nucleus and transcriptional activity of the NF-κB was finally confirmed by interrogating the expression level of the pro-survival genes (c-FLIP, Bcl-2) which was reduced by the cholesterol synthesis inhibitor Lovastatin (**Figure 6p, q**) as well as by the downregulation of TSPO (**Figure 1n, o**).

The final graphical model (**Figure 6r**) summarises this key step of this regulation, highlighting that the association of mitochondria with the nucleus relies on cholesterol-rich domains established by the retro-translocation of the prominent cholesterol binding protein TSPO.

Discussion

In this work, we demonstrate that mitochondria can establish point of contacts with the nucleus to favour spatially confined biochemical events that promote nuclear stabilization of pro-survival transcriptional factors such as the NF-κB. We also report that cholesterol works as an intermediate or a facilitator of the mitochondrial retro-communication together with Reactive Oxygen Species (ROS) and Ca^{2+} which have been acknowledged as the prevalent dynamic communicators between the two organelles[10,14].

The accumulation of cholesterol in the nucleus and nuclear envelope emerges as regulator of cellular reprogramming towards stress resistance and survival (**Fig. 6 f-m**). Even though cholesterol is known to affect transcription of genes[40] it is here for the first time reported to be trafficked into hot-spots at the interface between mitochondria and the nucleus to promote mito-nuclear communication, recapitulating other platforms of communications such as those between ER and Mitochondria (ER-MAMs)[41].

In response to mitochondrial re-organization, OMM based proteins such as TSPO may therefore deliver their lipid cargo, cholesterol, into the nuclear core of the cell where the concurrence of ROS may lead to auto-oxidative products of cholesterols (oxysterols[42]). The pattern of elements of the transduceome-complex[23], which all converge into the nucleus such as TSPO strongly argues for this (**SFigure 2 e-j**). We therefore feel to speculate that the fortification of the nuclear envelope with lipids such as cholesterol, rendering a change in the physical properties of diffusion and exchange of molecules **(Figure 6h)**, represents a crucial step in the altered transcriptional profile which enables aggressive cancer cells to differentiate from their less persistent counterparts.

While the observation that the mitochondrial interactome is crucial to cellular health is not new[43], the fine regulation of mitochondrial juxtaposition on the nucleus is. We have detailed that TSPO is required for this inter-organellar interaction, and in turn, its ligands are efficient

in pharmacologically modulating this interaction and movement of cholesterol (**Fig. 5**). Disruption of the known partners such as ACBD3 just partially affects the inter-organellar contacting, suggesting that the tethering capacity is relying on TSPO (**Fig. 5a-f**).

TSPO is an ancient protein[44] and its key part in the physical fine-tuning between two genomes may be an evolutional adaptation taking place via the exploitation of a lipid binding protein to fulfil both an anatomical and functional interaction.

In cellular models of malignant diseases, such as breast cancer derived lines such as MDA cells, NAM are prominent, far more than in the less aggressive counterpart MCF-7 cells. In MCF-7 cells, STS treatment is nonetheless able to promote a statistically significant gain in distance between mitochondria and nucleus (**Fig. 3 I, j**) even though still not within the range of contacts as it does in the MDA cells in which TSPO is very high (**Fig. 4 a,b**). This steady-state formation of NAM may be an 'already established' communication platform in these cells which is exacerbated by cholesterol dysregulation.

NAM will in turn increase the exposure of the nucleus to hydrogen peroxide (H_2O_2), superoxide (O_2^-) as well as hydroxyl radical (OH^-) generated in excess by defective mitochondria, as in those overexpressing TSPO. The nucleus is usually out of reach of mitochondrial O_2^- and OH^- which have very low estimated diffusion co-efficients[45]. However, the formation of NAM would bring mitochondria within angstroms range to the nuclear DNA facilitating the exposure of reactive species to the nuclear DNA[46] along with the accumulation of the NF-κB[14].

NAM may therefore represent both a defensive mechanism in response to apoptotic cues in the short term as well as a detrimental coupling which compromises DNA integrity in the long one, leading to genomic alterations. This ties well into the observations that cytoskeletal reorganization (which we have not here investigated) and cellular morphology are key factors in cellular resistance to apoptosis as well as in regulating the NF-κB signalling[47,48].

Equally, nuclear pleomorphism of tumours, proposed as a biomarker of malignancy for breast cancer[49], and the associated somatic mutations could be the consequence of the continuous exploitation of this localised, but nuclear-focused, stress signalling.

Mitochondrial repositioning is nonetheless secondary to inefficient mitochondrial quality control for impaired mitophagy[50], which causes the accumulation of inefficient organelles and their bypassed respiratory products. TSPO suppresses PINK1-PARKIN driven mitophagy by impairing the ubiquitination of proteins[21] and the mitochondria which overexpress TSPO are therefore prone to repositioning on the nucleus, as they are able to systematically evade control by autophagy. The previously described de-ubiquitinating properties of TSPO[22], lead us to speculate that trafficking of TSPO onto the nuclear envelope could replicate a similar outcome in the nucleus by preventing nucleophagy[51] of which the undulated nuclear envelope observed ultra-structurally (**SFigure 2 a,b**) could be the consequence. The alteration in lipid composition of the membranes to which TSPO localises (mitochondria) or re-localises (nucleus) could be also instrumental for this as well as to the altered organellar life cycle and protein interactome (**Figure 5h**). Mitochondrial network remodelling, cholesterol sequestration on the perinuclear region and cell death evasion are indeed avoidable by the downregulation of TSPO, its pharmacological inhibition as well as the pharmacological activation of mitophagy. Furthermore, TSPO is overexpressed in mammary gland cell lines that have developed resistance to ET thus conferring resistance to those who might instead be susceptible to the treatment (**Figure 3 d-g**). Overexpression of the ΔTSPO-CRAC mutant, which fails binding of cholesterol by TSPO, is unable to replicate the same effect (**Figure 5 g**). These experiments propose therefore a critical role for cholesterol in the resistance behaviour primed by the MRR, which is executed by physical re-organization of the mitochondrial network on the nucleus to via specific contacts, which have been here reported for the first time.

Author Contribution

M.C. conceived, designed and coordinated the project together with R.D, and D.A.E. M.C. R.D., L.H., D.A.E, J.C., D.F., M. S. A. performed the experiments and ran the analysis. R.F., G.V and L.A performed the EM analysis whilst G. T., M.M. the immunohistochemistry analysis on which guidance was obtained by K.S and V.Z., R.B. and G.S. worked out the bioinformatics data.

All authors have critically reviewed the manuscript and advised accordingly.

Acknowledgments

The research activities lead by M.C. are supported by the following funders, who are gratefully acknowledged: Biotechnology and Biological Sciences Research Council [grant numbers BB/M010384/1 and BB/N007042/1]; Bloomsbury Colleges Consortium PhD Studentship Scheme; The Petplan Charitable Trust; Umberto Veronesi Foundation; Marie Curie Actions and LAM-Bighi Grant Initiative. FIRB-Research Grant Consolidator Grant 2 [grant number: RBFR13P392], Italian Ministry of Health [IFO14/01/R/52].

Conflict of Interest

This research was conducted in the absence of any commercial or financial relationships that could be construed as a potential conflict of interest.

Methods

Immunohistochemistry/Immunocytochemistry*:* Immunofluorescence: Cells were fixed in 4% PFA (10 mins, RT) followed by 3 five-minute washes in PBS. Permeabilization was performed with 0.5% Triton-X in PBS (10 mins, RT) followed by washing. Blocking was carried out for 1h at RT in 10% Goat Serum and 3% BSA in PBS. Primary antibody incubations were conducted overnight for 16 h at 4˚C in blocking solution as described. After a further wash step, secondary antibodies were incubated for 1 h in blocking solution, before a final wash step. Cells were then mounted on slides with DAPI mounting medium (Abcam, ab104139). Cells were stained with the following primary antibodies: ATPB (Abcam ab14730) 1:400, Lamin B2 (Abcam ab8983) 1:500; TSPO (Abcam, ab109497) 1:200, NF-kB (AbCam, ab16502) 1:500, 1:1000 ATAD3 (Gift from Dr Ian Holt, Biodonista, 1:400 LXRβ (Abcam ab28479), 1:500 STAR (AbCam ab58013); and the following secondary antibodies: α-mouse Alexa 555 (Life Technologies, A21424) 1:1000; α-rabbit Alexa 488 (Life Technologies, A11008) 1:1000.

Single dye immunofluorescence was used to stain paraffin sections of human mammary tissues with different TSPO antibody (ab109497) / NF-kB (ab32360). The binding of mouse primary antibodies was detected using Alexa Fluor 488 (or 594) fluorochrome-conjugated goat anti-mouse IgG. Tissue sections were mounted with Floroshield Mounting Medium with DAPI to show

Cell Culture*:* Human mammary cell lines MDA-MB-231 and MCF7 canine mammary line CF41 and feline mammary line K248P, were maintained at 37˚C under humidified conditions and 5% CO_2 and grown in Dulbecco's modified Eagle medium (Life Technologies, 41966-052) supplemented with 10% foetal bovine serum (Life Technologies, 10082-147), 100 U/mL penicillin, and 100 mg/mL streptomycin (Life Technologies, 15140-122). K248P cells were additionally supplemented with 10 µg/ml insulin (sigma-aldrich). Cells were transiently

transfected with genes of interest or siRNA using a standard Ca^{2+} phosphate method as described previously[51] or using manufacturers' instructions for Lipofectamine 3000 (Thermofisher 18324010).

***Cell Fractionation**:* Cells were lysed in cold isotonic buffer (250 mM Sucrose, 10 mM KCl, 1.5 mM $MgCl_2$, 1 mM EDTA, 1 mM EGTA, 20 mM HEPES, pH 7.4) containing protease inhibitor cocktail (Roche, 05892791001) by passing through a 26-gauge needle 10 times using a 1 ml syringe, followed by 20 minutes incubation on ice. Nuclei were separated by centrifugation at 800g for 5 minutes at 4°C. For nuclear fractions, pellets were washed once in isotonic buffer followed by centrifugation 800g for 10 minutes at 4°C. Pellets were suspended in standard lysis buffer (150 mM NaCl, 1% v/v Triton X-100, 20 mM Tris pH 7.4) plus 10% glycerol and 0.1% SDS and sonicated for 5 seconds to dissolve pellet. For mitochondrial fractions, supernatants were transferred to fresh tubes and centrifuged at 10000g for 10 minutes at 4°C, Subsequent supernatants were collected as the cytosolic fractions while mitochondrial pellets were washed once in cold isotonic buffer then centrifuged at 10000g for 10 minutes at 4°C. Finally, mitochondrial pellets were lysed in lysis for 30 minutes on ice.

***Western Blot**:* Sample proteins were quantified using a BCA protein assay kit (Fisher Scientific, 13276818). Equal amounts of protein (10-30 µg for whole cell lysates/cytosolic fractions; 10 µg for mitochondrial. Nuclear fractions) were resolved on 12% SDS-PAGE gels and transferred to nitrocellulose membranes (Fisher Scientific, 10339574). The membranes were blocked in 3% non-fat dry milk in TBST (50 mM Tris, 150 mM NaCl, 0.05% Tween 20, pH 7.5) for 1 h then incubated with the appropriate diluted primary antibody at 4˚C overnight: LC3 (Abcam, ab48394) 1:1000; TSPO (Abcam, ab109497) 1:5000; Actin (ab8266). 1:2000; ATPB (Abcam, ab14730) 1:5000, BAX (Abcam, ab32503) 1:1000; CytC (ab13575) 1:1000; Histone H3 (ab8580) 1:1000 NF-kB (ab32360 1:1000; Lamin B1 (ab16048) 1:1000; MTCO1 (ab14705) 1:1000. Membranes were washed in TBST (3 x 15 mins at RT) and then incubated with corresponding peroxidase-conjugated secondary antibodies (Dako, P0447,

P0448) for 1h at RT. After further washing in TBST, blots were developed using an ECL Plus western blotting detection kit (Fisher Scientific, 12316992). Immunoreactive bands were analyzed by performing densitometry with ImageJ software.

Confocal Imaging/ImageJ*:* Fluorescent labeling was observed through a LSM 5 Pascal confocal microscope (Zeiss, Oberkochen, Germany) and images were recorded with the Pascal software (Zeiss). All image analysis was done using Fiji (ImageJ; NCBI, USA) and corresponding plug-ins. All staining was checked for non-specific antibody labeling using control samples without primary antibody. None of the controls showed any signs of nonspecific fluorescence. For ICC and IHC imaging, single optical sections were analyzed. The infiltrate analysis was done using orthogonal rendering 3D optical stacks and counting the number of infiltrates per cell nucleus. The mitochondrial network analysis was performed using the 'skeletonize' plugin. Higher resolution airyscan processed images were acquired using an LSM 880 Confocal with Airyscan (Carl Zeiss, Jena, Germany) system with GaAsP detectors and a module for airyscan imaging. In Airyscan modes, a 63x Plan Apochromat (1.4 NA) oil objective was used. Confocal imaging was sequential for different fluorophore channels to obtain a series of axial images. Images of cells were optimized for visualization by manually adjusting the minimum and maximum intensity values of the histogram in the Zen software (Carl Zeiss). Images were analyzed using the variance filter and quantified by co-localization of fluorophores.

Cell Proliferation assays*:* Cell proliferation assay were performed using the WST-1 Cell Proliferation Assay Kit (ab65473) and assessed on a standard plate reader (Tecan SUNRISE)

Cell Death Assays*:* Cells were fixed in 4% PFA for 10 mins at, RT followed by 3 five-minute washes in PBS. Permeabilization was performed with 0.2% Triton-X100 in PBS for 10 mins at RT followed by washing. Death assays TUNEL Assay Kit - *in situ* Direct DNA Fragmentation (ab66108) as per the manufacturer's instructions. Alternatively, cells were live

stained with Hoechst 33342 (Sigma H6024) and Propidium iodide (Sigma 25535) to mark apoptosing cells and imaged on an inverted fluorescence microscope.

Fluorescence imaging*:* Cells were incubated with 5 μM dihydroethidium (DHE, Life Technologies, D-1168) or 5 μM MitoSOX (Life Technologies, M-36008) in recording media (125 mM NaCl, 5 mM KCl, 1 mM NaH_2PO_4, 20 mM HEPES, 5.5 mM glucose, 5 mM $NaHCO_3$, and 1 mM $CaCl_2$, pH 7.4) for 30 minutes at 37 ^{0}C. Cells were washed once in recording medium then transferred to a Leica SP-5 confocal microscope (63X oil objective lens) for imaging and fluorescence intensity was measured through continuous recording for at least 10 mins. Settings were kept constant between experiments. Mitochondrial ROIs were selected, and the corresponding fluorescence intensities calculated. For the transport of cholesterol assay, Ergosta (dehydroergosterol- ergosta-5,7,9(11),22-tetraen-3β-ol) was prepared and loaded as previously described[52]. Briefly, Ergosta was added to an aqueous solution of MβCD (3mM Ergosta and 30mM MβCD). This mixture was overlaid with nitrogen, continuously vortexed under light protection for 24 h at room temperature and filtered through a 0.2 μm filter to remove insoluble material and Ergosta crystals. Then, 20 μg of DHE was added to the cells in the form of DHE-MβCD complexes and allowed to incubate for 90 minutes at room temperature in PBS. Prior to imaging, cells were washed three times with culture media before being incubated with 20 nM MitoTracker™ Red CMXRos. Cell were washed and then imaged.

Statistical analysis: Data are presented as mean ± standard deviation of the mean. One-way analysis of variance (ANOVA) was used in multiple group comparisons with Bonferroni's *post hoc* test to compare two data sets within the group and a *p* value less than 0.05 was considered significant. All analyses were performed in Microsoft Office Excel 2010 and GraphPad Prism 7. *p = <0.05, **p = <0.01, ***p = <0.001

Preparation of cells for Electron Microscopy (TEM and Immunogold TEM)

For TEM analysis, MDA-MB-231 cells (control and treated with 0.5 μm for 16 h) were fixed at room temperature with 2.5% glutaraldehyde (v/v) in 0.1 M sodium cacodylate buffer (pH 7.4)

for 3 h. The cells were pelleted by centrifugation, washed in buffer and post-fixed for 1 h with 1% osmium tetroxide in 0.1 M sodium cacodylate buffer. Samples were thoroughly rinsed, dehydrated in a graded series of ethanols and embedded in epoxy resin (TAAB 812). Ultrathin sections (70-90 nm) were cut using a Leica UC7 ultramicrotome mounted on 150 mesh copper grids and contrasted using Uranyless (TAAB) and 3% Reynolds Lead citrate (TAAB). Sections were examined at 120kV on a JEOL JEM-1400Plus TEM fitted with a Ruby digital camera (2kx2k). For TEM immunogold labelling, cell samples were fixed with 4% (w/v) paraformaldehyde, 0.1% (v/v) glutaraldehyde in 0.1M phosphate buffer (pH 7.4) for 4 h at room temperature and spun down on 20% gelatine. Gelatine cell pellets were cryoprotected by incubating in 2.3M sucrose overnight at 4°C. Gelatine blocks containing cells were cut further into 1-2mm cubes, mounted on aluminium pins and cryofixed by plunging into liquid nitrogen. Samples were stored in liquid nitrogen prior to cryosectioning. Ultrathin sections (70-90 nm thick) were cut using a Leica EM FC6 cryo-ultramicrotome and mounted on pioloform film-supported nickel grids according to the Tokuyasu method (1). Sections were immunolabeled using anti-TSPO (Abcam, ab109497) (1:200) followed by a 12nm-colloidal gold anti-rabbit secondary antibody (Jackson ImmunoResearch) (1:40). Grids were examined at 120 kV on a JEOL JEM-1400Plus TEM fitted with a Ruby digital camera (2kx2k).

Table 1: Chemical Structures of the Compounds Used

Compound	IUPAC	Structure
PK11195	1-(2-Chlorophenyl)-N-methyl-N-(1-methylpropyl)-3-isoquinolinecarboxamide;	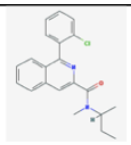
FGIN (FGIN-1-27)	N, N-Dihexyl-2-(4-fluorophenyl) indole-3-acetamide	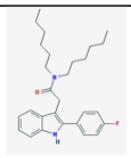
Ro5 (Ro5-4864)	7-chloro-5-(4-chlorophenyl)-1-methyl-3H-1,4-benzodiazepin-2-one	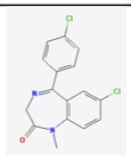
Staurosporine	(2S,3R,4R,6R)-3-methoxy-2-methyl-4-(methylamino)-29-oxa-1,7,17-triazaoctacyclo [12.12.2.1^{2,6}.0^{7,28}.0^{8,13}.0^{15,19}.0^{20,27}.0^{21,26}] nonacosa-8,10,12,14,19,21,23,25,27-nonaen-16-one	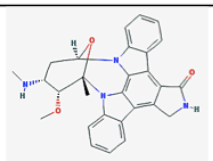
Doxorubicin	(7S,9S)-7-[(2R,4S,5S,6S)-4-amino-5-hydroxy-6-methyloxan-2-yl] oxy-6,9,11-trihydroxy-9-(2-hydroxyacetyl)-4-methoxy-8,10-dihydro-7H-tetracene-5,12-dione	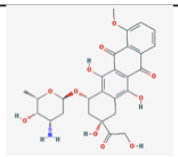
Vincristine	methyl (1R,9R,10S,11R,12R,19R)-11-(acetyloxy)-12-ethyl-4-[(13S,15S,17S)-17-ethyl-17-hydroxy-13-(methoxycarbonyl)-1,11-diazatetracyclo[13.3.1.0^{4},^{12}.0^{5},^{10}]nonadeca-4(12),5,7,9-tetraen-13-yl]-8-formyl-10-hydroxy-5-methoxy-8,16-diazapentacyclo[10.6.1.0^{1},^{9}.0^{2},^{7}.0^{16},^{19}]nonadeca-2,4,6,13-tetraene-10-carboxylate	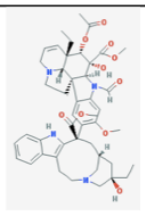
Tamoxifen	(2-{4-[(1Z)-1,2-diphenylbut-1-en-1-yl] phenoxy}ethyl)dimethylamine	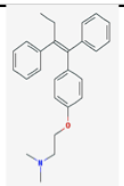

References

1 Topf, U. *et al.* Chatty Mitochondria: Keeping balance in cellular protein homeostasis. *Trends in Cell Biology* **26**, 577-586, https://doi.org/10.1016/j.tcb.2016.03.002 (2016).

2 Guha, M. *et al.* Mitochondrial retrograde signaling induces epithelial-mesenchymal transition and generates breast cancer stem cells. *Oncogene* **33**, 5238-5250, doi:10.1038/onc.2013.467 (2014).

3 Butow and Avadhani. Mitochondrial Signalling: The Retrograde Response. *Molecular Cell* **14,** 1-15, https://doi.org/10.1016/S1097-2765(04)00179-0 (2004).

4 Carden, T., Singh, B., Mooga, V., Bajpai, P. & Singh, K. K. Epigenetic modification of miR-663 controls mitochondria-to-nucleus retrograde signaling and tumor progression. *J Biol Chem*, doi:10.1074/jbc.M117.797001 (2017).

5 Feske, S. *et al.* Ca^{2+}/calcineurin signalling in cells of the immune system. *Biochem and Biophys Res Comms* **311,** 1117-1132, https://doi.org/10.1016/j.bbrc.2003.09.174 (2003).

6 Nguyen, V. T. *et al.* Differential epigenetic reprogramming in response to specific endocrine therapies promotes cholesterol biosynthesis and cellular invasion. *Nat Commun* **6**, 10044, doi:10.1038/ncomms10044 (2015).

7 Magnani, L. *et al.* Acquired CYP19A1 amplification is an early specific mechanism of aromatase inhibitor resistance in ERalpha metastatic breast cancer. *Nat Genet* **49**, 444-450, doi:10.1038/ng.3773 (2017).

8 Hardwick, M. *et al.* Peripheral-type benzodiazepine receptor (PBR) in human breast cancer: correlation of breast cancer cell aggressive phenotype with PBR expression, nuclear localization, and PBR-mediated cell proliferation and nuclear transport of cholesterol. *Cancer Res* **59**, 831-842 (1999)

9 Fan, J. & Papadopoulos, V. Evolutionary origin of the mitochondrial cholesterol transport machinery reveals a universal mechanism of steroid hormone biosynthesis in animals. *PLoS One* **8**, e76701, doi:10.1371/journal.pone.0076701 (2013).

10 Quiros, P. M., Mottis, A. & Auwerx, J. Mitonuclear communication in homeostasis and stress. *Nat Rev Mol Cell Biol* **17**, 213-226, doi:10.1038/nrm.2016.23 (2016).

11 De Stefani, D. *et al.* VDAC1 selectively transfers apoptotic Ca2+ signals to mitochondria. *Cell Death Differ* **19**, 267-273, doi:10.1038/cdd.2011.92 (2012).

12 Wallace, D. C. Mitochondria and cancer. *Nat Rev Cancer* **12**, 685-698, doi:10.1038/nrc3365 (2012).

13 Rizzuto, R., De Stefani, D., Raffaello, A. & Mammucari, C. Mitochondria as sensors and regulators of calcium signalling. *Nat Rev Mol Cell Biol* **13**, 566-578, doi:10.1038/nrm3412 (2012).

14 Monaghan, R. M. *et al.* A nuclear role for the respiratory enzyme CLK-1 in regulating mitochondrial stress responses and longevity. *Nat Cell Biol* **17**, 782-792, doi:10.1038/ncb3170 (2015).

15 Miettinen, H. et al. Expression of peripheral-type benzodiazepine receptor and diazepam binding inhibitor in human astrocytomas: relationship to cell proliferation. Cancer Res **55**, 2691-2695 (1995).

16 Beinlich, A., Strohmeier, R., Kaufmann, M. & Kuhl, H. Relation of cell proliferation to expression of peripheral benzodiazepine receptors in human breast cancer cell lines. Biochem Pharmacol **60**, 397-402 (2000).

17 Maaser, K. et al. Up-regulation of the peripheral benzodiazepine receptor during human colorectal carcinogenesis and tumor spread. Clin Cancer Res **11**, 1751-1756, doi:10.1158/1078-0432.CCR-04-1955 (2005).

18 Rone, M. B., Fan, J. & Papadopoulos, V. Cholesterol transport in steroid biosynthesis: role of protein-protein interactions and implications in disease states. Biochim Biophys Acta1791, 646-658, doi:10.1016/j.bbalip.2009.03.001 (2009).

19 Rone, M. B. et al. Identification of a dynamic mitochondrial protein complex driving cholesterol import, trafficking, and metabolism to steroid hormones. Mol Endocrinol 26, 1868-1882, doi:10.1210/me.2012-1159 (2012).

20 Papadopoulos, V. et al. Translocator protein-mediated pharmacology of cholesterol transport and steroidogenesis. Mol Cell Endocrinol **408**, 90-98, doi:10.1016/j.mce.2015.03.014 (2015).

21 Gatliff, J. & Campanella, M. TSPO is a REDOX regulator of cell mitophagy. Biochem Soc Trans **43**, 543-552, doi:10.1042/BST20150037 (2015).

22 Gatliff, J. et al. TSPO interacts with VDAC1 and triggers a ROS-mediated inhibition of mitochondrial quality control. Autophagy **10**, 2279-2296, doi:10.4161/15548627.2014.991665 (2014).

23 Gatliff, J. et al. A role for TSPO in mitochondrial Ca(2+) homeostasis and redox stress signaling. Cell Death Dis **8**, e2896, doi:10.1038/cddis.2017.186 (2017).

24 Zheng, J. et al. Differential expression of the 18 kDa translocator protein (TSPO) by neoplastic and inflammatory cells in mouse tumors of breast cancer. Mol Pharm **8**, 823-832, doi:10.1021/mp100433c (2011).

25 Gatliff, J. & Campanella, M. The 18 kDa translocator protein (TSPO): a new perspective in mitochondrial biology. Current molecular medicine **12**, 356-368 (2012).

26 Tang, D. et al. Preclinical Evaluation of a Novel TSPO PET Ligand 2-(7-Butyl-2-(4-(2-[(18)F]Fluoroethoxy)phenyl)-5-Methylpyrazolo[1,5-a]Pyrimidin-3 -yl)-N,N-Diethylacetamide ((18)F-VUIIS1018A) to Image Glioma. Mol Imaging Biol, doi:10.1007/s11307-018-1198-7 (2018).

27 Tantawy, M. N. et al. Translocator Protein PET Imaging in a Preclinical Prostate Cancer Model. Mol Imaging Biol **20**, 200-204, doi:10.1007/s11307-017-1113-7 (2018).

28 Herrero-Martin, G. & Lopez-Rivas, A. Statins activate a mitochondria-operated pathway of apoptosis in breast tumor cells by a mechanism regulated by ErbB2 and dependent on the prenylation of proteins. FEBS Lett **582**, 2589-2594, doi:10.1016/j.febslet.2008.06.034 (2008).

29 Khan, S., Lopez-Dee, Z., Kumar, R. & Ling, J. Activation of NFkB is a novel mechanism of pro-survival activity of glucocorticoids in breast cancer cells. Cancer Lett **337**, 90-95, doi:10.1016/j.canlet.2013.05.020 (2013).

30 Ling, J. & Kumar, R. Crosstalk between NFkB and glucocorticoid signaling: a potential target of breast cancer therapy. Cancer Lett 322, 119-126, doi:10.1016/j.canlet.2012.02.033 (2012).

31 East, D. A. et al. PMI: a DeltaPsim independent pharmacological regulator of mitophagy. Chem Biol 21, 1585-1596, doi:10.1016/j.chembiol.2014.09.019 (2014).

32 Georgakopoulos, N. D. et al. Reversible Keap1 inhibitors are preferential pharmacological tools to modulate cellular mitophagy. Sci Rep 7, 10303, doi:10.1038/s41598-017-07679-7 (2017).

33 Jaremko, L., Jaremko, M., Giller, K., Becker, S. & Zweckstetter, M. Structure of the mitochondrial translocator protein in complex with a diagnostic ligand. Science 343, 1363-1366, doi:10.1126/science.1248725 (2014).

34 Tenev, T. *et al.* The Ripoptosome, a signaling platform that assembles in response to genotoxic stress and loss of IAPs. *Mol Cell* **43**, 432-48. doi: 10.1016/j.molcel.2011.06.006. (2011).

35 Jeng, M. H. et al. Estrogen receptor expression and function in long-term estrogen-deprived human breast cancer cells. Endocrinology **139**, 4164-4174, doi:10.1210/endo.139.10.6229 (1998).

36 Santen, R. J., Lobenhofer, E. K., Afshari, C. A., Bao, Y. & Song, R. X. Adaptation of estrogen-regulated genes in long-term estradiol deprived MCF-7 breast cancer cells. Breast Cancer Res Treat **94**, 213-223, doi:10.1007/s10549-005-5776-4 (2005).

37 Marwarha, G., Raza, S., Hammer, K. & Ghribi, O. 27-hydroxycholesterol: A novel player in molecular carcinogenesis of breast and prostate cancer. Chem Phys Lipids **207**, 108-126, doi:10.1016/j.chemphyslip.2017.05.012 (2017).

38 Kloudova, A., Guengerich, F. P. & Soucek, P. The Role of Oxysterols in Human Cancer. Trends Endocrinol Metab **28**, 485-496, doi:10.1016/j.tem.2017.03.002 (2017).

39 Modzel, M., Lund, F. W. & Wustner, D. Synthesis and Live-Cell Imaging of Fluorescent Sterols for Analysis of Intracellular Cholesterol Transport. Methods Mol Biol **1583**, 111-140, doi:10.1007/978-1-4939-6875-6_10 (2017).

40 Bovenga, F., Sabba, C. & Moschetta, A. Uncoupling nuclear receptor LXR and cholesterol metabolism in cancer. *Cell Metab* **21**, 517-526, doi:10.1016/j.cmet.2015.03.002 (2015).

41 Tambini, M. D. et al. ApoE4 upregulates the activity of mitochondria-associated ER membranes. *EMBO Rep* **17**, 27-36, doi:10.15252/embr.201540614 (2016).

42 Murphy and Johnson. Cholesterol, Reactive Oxygen Species, and the formation of biologically active mediators. *J Bio Chem* **283,** 15521-15525, doi: 10.1074/jbc.R700049200 (2008).

43 Nunnari and Suomalainen. Mitochondria: In Sickness and in Health. *Cell* **148**, 1145-1159, DOI:https://doi.org/10.1016/j.cell.2012.02.035 (2012).

44 Fan, J. *et al.* Structural and functional evolution of the translocator protein (18 kDa). *Curr Mol Med* **12**, 369–386 (2012).

45 Cardoso, A. R. et al. Mitochondrial compartmentalization of redox processes. Free Radic Biol Med **52**, 2201-2208, doi:10.1016/j.freeradbiomed.2012.03.008 (2012).

46 Ishikawa, K. *et al.* ROS-generating mitochondrial DNA mutations can regulate tumor cell metastasis. *Science* **320**, 661-664, doi:10.1126/science.1156906 (2008).

47 Spencer, W. *et al.* Taxol selectively blocks microtubule dependent NF-kappaB activation by phorbol ester via inhibition of IkappaBalpha phosphorylation and degradation. *Oncogene* **18**, 495-505, doi:10.1038/sj.onc.1202335 (1999).

48 Becker-Weimann, S. *et al.* NFkB disrupts tissue polarity in 3D by preventing integration of microenvironmental signals. *Oncotarget* **4**, 2010-2020, doi:10.18632/oncotarget.1451 (2013).

49 Bussolati, G., Marchio, C., Gaetano, L., Lupo, R. & Sapino, A. Pleomorphism of the nuclear envelope in breast cancer: a new approach to an old problem. *J Cell Mol Med* **12**, 209-218, doi:10.1111/j.1582-4934.2007.00176.x (2008)

50 Twig, G and Shirihai, OS. The interplay between mitochondrial dynamics and mitophagy. *Antioxid Redox Signal* **14,** 1939-1951, DOI: 10.1089/ars.2010.3779 (2011).

51 Dou, Z. *et al.* Autophagy mediates degradation of nuclear lamina. *Nature* **527**, 105-109, doi:10.1038/nature15548 (2015).

52 Morelli, A. *et al.* Extracellular ATP causes ROCK I-dependent bleb formation in P2X7-transfecyed HEK293 cells. *Mol Biol Cell* **14**, 2655-2664, doi:10.1091/mbc.02-04-0061 (2003).

53 McIntosh, A. L. *et al.* Fluorescence techniques using dehydroergosterol to study cholesterol trafficking. *Lipids* **43**, 1185-1208, doi:10.1007/s11745-008-3194-1 (2008).

Legends to Figures

Figure 1: TSPO expression which positively associates with breast cancer aggressiveness drives NF-κB nuclear recruitment

(a) Pseudo-coloured images of fluorescent immunohistochemistry using anti-TSPO antibody reveals higher expression in human mammary cancer tissue compared with healthy.

(b) Quantification of TSPO signal normalised to DAPI staining, shows difference between the cancerous cells and healthy tissue is statistically significant (Healthy 8.18±2.4; Benign 24.54±5.2; Malignant 40.31±2.7; n=10; $p<0.05$, 0.01).

(c) Comparison of TSPO expression in human mammary tumours using microarray data from the TCGA breast cancer database.

(d) Confocal imaging of fluorescence immunohistochemistry from primary human tissue samples of varying degrees of cancer labelled for NFkB (yellow) and nuclear dye DAPI (blue) shows increased expression and translocation of NF-kB into nucleus in malignant samples.

(e) The intensity of NF-kB- immunohistochemistry shows significant increased labelling in malignant tissue compared with benign and healthy tissue (Healthy 43.288±10.6; Benign 54.17±12.7; Malignant 75.94±10.7; n=60 $p<0.001$)

(f) Comparison of NF-kB expression in human mammary tumours using microarray data from the TCGA breast cancer database.

(g) Immunohistochemistry of MCF-7 and MDA-MB-231 with DAPI (blue) TSPO (green) and ATPB (red) showing higher expression of TSPO in MDA-MB-231 cells.

(h) Western blot of TSPO in MBA-MB-231 and MCF-7 cells (N=4).

(i) Normalized quantification of TSPO signal in western blots shows higher expression in MDA-MB-231 compared to MCF-7 cells (5.404004 ± 1.491815, $p<0.05$) n=3).

(j) Western blot analysis of NF-kB concentration in the cytosolic and nuclear fractions following STS treatment. Nuclear translocation is significantly reduced in -TSPO cells.

(k) Quantification of cytosolic NF-κB normalised to beta-actin in control and -TSPO cells treated with STS (Control – STS normalised 1; Control + STS 0.935±0.793; - TSPO – STS 1.193±0.895; -TSPO + STS 0.841±0.567; n=3 $p>0.05$).

(l) Quantification of nuclear NF-κB normalised to Lamin B1 in control and -TSPO cells treated with STS (Control – STS normalised 1; Control + STS 2.577±1.557; - TSPO – STS 0.193±0.062; -TSPO + STS 0.435±0.277; n=3 $p<0.05$, $p<0.01$, $p<0.001$).

(m) Confocal images of fluorescence immunohistochemistry on MDA-MB-231 cells labelled for DAPI (blue), NFκB (green) and ATPB (red), treated with STS, PMI and STS+PMI.

(n) Reduced Bcl-2 mRNA expression in -TSPO MDA-MB-231 (Control normalised 1; Control + STS 1.50±0.065; -TSPO 0.68±0.02; -TSPO + STS 0.9±0.04; n=3; $p<0.01$)

(o) Reduced c-FLIP mRNA expression in -TSPO MDA-MB-231 (Control normalised 1; Control + STS 1.5±0.04; -TSPO 0.75±0.03; -TSPO + STS 0.89±0.02; n=3; $p<0.01$)

(p) Intensity graphs of percentage of nuclear NFKB shows significant translocation with STS treatment which is reduced when PMI is introduced (Control 18.42±4.17; PMI 41.39±9.09; STS 18.57±4.7; PMI + STS 30.08±7.8; n=30; $p<0.001$).

(q) Western blot analysis of Bcl2 in control and –TSPO MDA-MB-231 cells following STS treatment. Bcl2 upregulation is not observed in STS treated TSPO knockdown cells.

Figure 2: TSPO confers resistance to apoptosis

(a) Immunocytochemistry of MDA-MB-231 with DAPI (red), NF-kB (Cyanin) in control cells, exposed to STS in absence or presence of TSPO ligand PK11195.

(b) Quantification of NF-kB signal in the nucleus following STS combined with PK11195. (Control 26.86±15.02; PK11195 21.26±12.24; STS 49.36±23.52; PK + STS 34.52±21.36; n=15 $p<0.05$, $p<0.01$, $p<0.001$)

(c) Quantification of NF-kB signal in the nucleus following STS combined with Pravastatin (PVS). (Control 25.14±14.78; PVS 25.70±17.88; STS 36.20±26.64; PVS + STS 32.59±21.00; n=10 $p<0.05$, $p<0.001$)

(d) Assessment of TSPO role in MDA-MB-231 cells constitutively knocked-down for NF-kB which show greater susceptibility to STS with no role for TSPO (NF-KB Ko 1.3±0.69; NF-KBKo +STS 38.18±4.04; -TSPO NFKBKo 2.88±0.07; -TSPO NFKBKo+STS 37.1±3.45; n=3; $p<0.05$).

(e) TUNEL assay of control and -TSPO cells exposed to STS reporting tangible differences (Control 1.37±.27; Control +STS 47.38±2.74; -TSPO 7.19 ±0.85; -TSPO + STS 61.25 ±2.06; n=3; $p<0.01$).

(f) Proliferation assay highlights differences in control and -TSPO cells at 72 hours post seeding ($p<0.01$).

(g) Western blotting of mitochondrial fraction (marked by ATPB) which reveals STS induced translocation of the pro-apoptotic BAX to be greater in -TSPO cells.

(h) Quantification of BAX signal normalised to ATPB (Control normalised 1; Control + STS 1.2 ± 0.18; -TSPO 2.35 ± .27; -TSPO + STS ±.48; n=3 $p<0.05$).

(i) Western blotting of cytosolic fraction (marked by Actin) which reveals STS induced translocation of the Cytochrome C (Cyt-C) in -TSPO cells.

(j) Intensity of Cyt C signal normalised to Actin is statistically quantified and put in histogram (Control normalised 1; Control + STS 1.82±.06; -TSPO 1.27± 0.032; -TSPO + STS 2.79 ± 0.18636; n=3; $p<0.05$).

(k) TSPO ligands PK11195, FGIN and Ro-5 exacerbate STS induced cell death in MDA-MB-231 cells (Untreated 3.71± 0.94548; Control 49.98 ±0.84; PK11195 59.43±0.68; FGIN 62.41±1.4; Ro-5 62.16±1.57, n=3, $p<0.05$, 0.001).

(l) TSPO ligands mediate the same effect during Doxorubicin treatment (Untreated 5.9±1.52; Control 16.00±2.633; PK11195 32.7±7.03; FGIN 38.9±2.3; Ro-5 36.1±2.23; n=4; $p<0.05$) and (m) Vincristine induced cell death (Untreated 10.05±0.95; Control 15.61±0.67; PK11195 43.6±1.02; FGIN 36.54±1.41; Ro-5 33.53±3.13; n=3; $p<0.001$).

Figure 3: Cholesterol binding is pivotal to TSPO driven protection from apoptosis

(a) Sketch depicting wild type TSPO and TSPOΔCRAC constructs used to knock-in the protein into MCF-7 cells.

(b) Wild type TSPO confers resistance to STS into MCF-7 cells (0.2 μM 16 h), whereas TSPOΔCRAC does not (Control 29.86±8.48; +TSPO 15.37±4.6; +TSPOΔCRAC 2.21; n=5, $p<0.005$).

(c) Western blot shows that plasmid-based knock-in of TSPO at 48 h in MCF-7 cells which only slightly reduces at 72 hours.

(d) Western blot showing that long-term tamoxifen treated MCF-7 cells, which are more resistant to cell death (LTED) express higher levels of TSPO compared with parental cells and this expression is enhanced under Tamoxifen treatment.

(e) Intensity blots analysis of the LTED cells with and without Tamoxifen reports the significant differences of TSPO expression (MCF-7 Control Normalised 1; MCF-7+TAM 19.85±9.8; LTED Control 45.88±13.3; LTED + TAM 76.41±11.3; n=3; $p<0.05$, 0.01, 0.005)

(f) Confocal imaging of MCF7 and MCF7T cells immuno-labelled for DAPI (blue), ATPB

(red) and ERα (green). TSPO ligand FGIN-1-27 causes cytoplasmic retention of ERα in MCF7T cells, however this effect was not observed in the control MCF7 cell. I would include some zooms to show this more clearly

(g) Quantification of ERα nuclear to cytoplasm ratio following treatment with TSPO ligand FGIN-1-27. (MCF7 1.74±1.00, MCF7 + FGIN 1.92±1.18, MCF7T 2.45±1.63, MCF7T + FGIN 1.89±1.34, n=30, $p<0.001$).

(h) MCF7T cells show resistance to STS treatment in comparison to MCF7. FGIN-1-27 appears to have no effect on STS induced cell death in both cell lines (MCF7 Control 8.09±4.68, MCF7T Control 7.17±3.34, MCF7 + FGIN 11.65±4.22, MCFT + FGIN 17.33±14.58, MCF7 + STS 61.61±47.89, MCF7T + STS 34.38±33.31, MCF7 + FGIN + STS 64.56±44.49, MCF7T + FGIN + STS 41.11±39.71, n=3, $p<0.001$, $p<0.01$).

(i) Representative ultrastructural images of control vs STS treated MCF7 cells showing mitochondrial (M-yellow) remodelling towards the nucleus (N-blue). I would also show a lower power where you can see a whole nucleus, to help convince you have not cherry picked a particular area.

(j) Quantification of closest mitochondrial-nuclear distance (nm) showing reduced distance to a minimum of 50nm in treated MCF7 cells (n=1). Don't see how there can be no variance in the control data here.

Figure 4: Mitochondria associate with the Nucleus in TSPO rich cells

(a) MCF-7 (top row) and MDA-MB-231 (bottom row) cells labelled with DAPI (blue), nuclear envelope protein Lamin B (red) and TSPO (green) reveal enhanced proximity to nucleus of the TSPO +ve mitochondrial network in MDA-MB-231 which express greater overall amount of TSPO.

(b) TSPO signal co-location with Lamin B signal in MDA-MB-231 cells in confocal optical sections is quantified (MCF7 Normalised 1; MDA-MB-231 5.40±1.5; n=3; $p<0.0005$)

(c) Western blot analyses of TSPO translocation into the nucleus following cytotoxic treatments with STS and rotenone. Left, TSPO expression in the cytosolic fraction normalised to beta actin. Middle, perinuclear TSPO expression controlled to nuclear envelope protein lamin B1. Right, nuclear TSPO normalised to histone H3 showing TSPO translocation into the nuclear region during cellular stress.

(d) Intensity blot analyses of TSPO expression in cellular compartments. Left, TSPO/actin ratio in the cytosolic fraction (Control DMSO normalised to 1; STS 0.896±0.543; Rotenone 0.905±0.487; n=3, ns). Middle, TSPO/Lamin B1 ratio in perinuclear region (Control DMSO normalised to 1; STS 1.812±1.162; Rotenone 2.037±1.137; n=3, ns). Right,

TSPO/Histone H3 ratio in the nuclear fraction, showing significantly higher nuclear translocation following stressors (Control DMSO normalised to 1; STS 5.601±3.703; Rotenone 2.625±1.085; n=3 $p<0.05$).

(e) Ultrastructure images of control vs STS treated MDA-MB-231 cells confirming physical interaction of the mitochondria (M-yellow) with the nucleus (N-blue). STS treatment shows endoplasmic reticulum (ER) displacement and the formation of contact sites between the mitochondrial and nuclear membranes.

(f) Quantification of least mitochondrial-nuclear distance in control and STS treated MDA-MB-231 cells (Control 65.45±13.89; STS 21.75±1.19; n=15 $p<0.001$).

(g) Fluorescence intensity vs time plots showing -TSPO cells have less ROS compared with control ones as measured with dihydroethidium (DHE) fluorescence (n=6)

(h) Average DHE fluorescence confirming the lower cytoplasmic ROS levels in -TSPO cells (Control normalised 1; -TSPO 0.59±0.07; n=20; $p<0.05$).

(i) Average mitochondrial accumulation of MitoSox, reporting significantly lower mitochondrial ROS levels, in -TSPO cells (Control normalised 1; STS 0.73±0.04; n=20; $p<0.05$).

(j) Confocal imaging of MDA-MB-231 cells immuno-labelled for DAPI (blue), TSPO (green) and ATPB (red) exposed to STS, PMI or PMI+STS revealing collapse of the TSPO+ve mitochondrial network otherwise prevented by PMI (n=5).

(k) Calculation of the median distance of mitochondrial particles from the centre of the nucleus significantly changes after treatment of STS in control MDA-MB-231 the distance is 4.3 µm more than in STS treated MDA-MB-231 (Control 16.17±11.17; STS 11.678±6.988; n=9 $p<0.01$).

(l) Calculation of the mitochondrial infiltrates into the nucleus measured in orthogonal images of STS treated MDA-MB-231 cells in absence or presence of PMI (Control 2.33±1.3; STS 13.11±3.9; PMI 2.44±1.51; PMI±STS 8±2.7; n=10; $p<0.05$, 0.01).

Figure 5: TSPO is required for the formation of mito-nuclear contact sites

(a) Airyscan resolution confocal images of co-localisation of nuclear envelope (Lamin B - red) and mitochondria (ATPB – Green) in scrambled siRNA control and TSPO knockdown MDA-MB-231 breast cancer cells.

(b) Quantification of contact site area normalised to nuclear envelope length. Knocking down TSPO prevents mitochondrial-nuclear contact site formation in MDA-MB-231 cells (Control 0.3106±0.213; -TSPO 0.15623±0.03181; n=5, $p<0.01$).

(c) Airyscan super resolution confocal images of co-localisation of nuclear envelope (Lamin B - red) and mitochondria (ATPB – Green) in control and TSPO overexpressing mouse embryonic fibroblasts (MEF).

(d) Quantification of contact site area normalised to nuclear envelope length. Overexpressing TSPO increases mitochondrial-nuclear contact sites in comparison to control MEF cells (Control 0.16073±0.04767; +TSPO 0.2278±0.147, n=3 $p<0.05$).

(e) Representative ultrastructure images of control vs wild type TSPO overexpressing MEFs.

(f) Quantification of closest mitochondrial-nuclear distance in TSPO overexpressing MEFs in comparison to controls (n=1).

(g) Graph reporting on the protective effect against cell death gained by wild type TSPO, but not TSPOΔCRAC in MEFs exposed to STS (Wildtype 11.7449±10.1751; +TSPO 71.865±68.555; TSPOΔCRAC 22.243±18.977; n=2 $p<0.001$).

(h) Graphical representation showing nuclear and non-nuclear interactors of TSPO in order to identify proteins interacting during the formation of mitochondrial-nuclear contact sites.

(i) Confocal images of known TSPO interactor ACBD3 knockdown and wildtype MDA-MB-231 cells. Cells were co-transfected with CFP (blue) and stained for Lamin B2 (green) and TSPO (red) following treatment with STS.

(j) Quantification of lamin/TSPO co-localisation in confocal images. Knocking down ACBD3 in control cells reduces mitochondria-nucleus interactions in untreated cells. However, following STS treatment loss of ACBD3 does not significantly reduce lamin/TSPO co-localisation in comparison to wildtype cells.

(k) Confocal images of DAPI (blue), Lamin B (Green) and mitochondrial TOM20 (red). Silencing known tether protein VAPB in MDA-MB-231 cells does not prevent the formation of contact sites observed by co-localisation (yellow) of the nuclear envelope and mitochondria.

(l) Quantification of lamin B and TOM20 co-localisation normalised to nuclear area in scrambled siRNA and VAPB knockdown MDA-MB-231 cells. (Control $0.202081\pm7.259\times10^{-3}$; -VAPB $0.022475\pm8.125\times10^{-3}$; n=15, ns)

Figure 6: Redistribution of Cholesterol by TSPO partakes in mitochondrial retrograde response.

(a) Confocal images of immune-labelled MDA-MB-231 cells for TSPO treated with 7 ketocholesterol (7-KC) showing upregulation of the protein after treatment.

(b) Western blot confirming TSPO upregulation in MDA-MB-231 in response to 7-KC.

(c) Intensity plots show significant 7-KC induced upregulation of TSPO in and MDA-MB-231 cells treated with 7-KC (Control 94.861±6.5, 7-KC 136.59±6.76; n=3; $p<0.01$).

(d) Orthogonal images detail the increased TSPO positive (red/yellow) infiltrates into nucleus (blue) in 7-KC treated MDA-MB-231 cells compared to untreated ones.

(e) The number of TSPO positive infiltrates per cell is quantified in the same conditions (Control 4.22±2.9; 7-KC ±2.3; n=9; $p<0.005$).

(f) Confocal images of mt-RFP expressing MDA-MB-231 cells (red) stained with cholesterol marker Filipin (cyan) and labelled with anti-Lamin B (green) reporting reduced cholesterol in the perinuclear region in -TSPO cells (bottom row).

(g) Graph which quantifies the reduced intensity of cholesterol -measured in the nuclei- in -TSPO cells compared with control. (Control 10.56±1.56; 8.4±1.26; n=15; $p<0.005$)

(h) Confocal images of MDA-MB-231 cells following STS treatment stained with ANE dye (Di-4-ANEPPHQ) dye to indicate nuclear membrane stiffness and cholesterol composition. Under STS treatment, the nuclear envelope becomes more disordered shown by an increase in green fluorescence.

(i) Quantification of nuclear ANE green to red ratio is significantly increased following STS Treatment.

(j) Diagram reporting the redistribution of cholesterol from the nucleus following the tested TSPO ligands, PK11195 and Ro-5 (Control normalised 1; PK11195 0.86±0.008; Ro-5 0.54±0.039; n=3; $p<0.001$).

(k) Evaluation of nuclear cholesterol capacity in MEFs expressing either wild type TSPO or TSPOΔCRAC. The data shows the cholesterol binding capacity of TSPO is required for nuclear accumulation of cholesterol.

(l) Confocal live fluorescent images showing intracellular trafficking of cholesterol analogue, ergosta (dehydroergosterol – cyan) co-stained with mitotracker (red). TSPO ligand PK11195 prevents uptake of ergosta into the nucleus, similarly to cholesterol trafficking inhibitor U-18666A.

(m) Quantification of ergosta nuclear intensity in canine mammary cell line CF35 following treatments with PK11195 and U-18666A (Control 23.629±17.031; PK11195 9.784±5.814; U-18666A 12.164±5.362, n=25 $p<0.001$).

(n) Confocal images of MDA-MB-231 cells immuno-labelled for ATPB (Red) and corresponding skeletonized representation of mitochondrial network in PK11195, STS and PK11195 + STS co-treatment conditions.

(o) Quantification of mitochondrial branches per cell reveals that PK11195 treated cells

have far more arborizations retained also during STS treatment (Control 371.6±82.3; PK11195 532±123; STS 275±62.9; PK11195+STS 390±86.5; n=10; p<0.01, 0.005).

(p) Graph on the ability by the cholesterol synthesis inhibitor Lovastatin to significantly reduce mRNA expression Bcl2 after treatment with STS as (Control normalised 1; control + STS 1.08±0.04; lovastatin 0.6±0.18; lovastatin+STS 0.77±0.2; n=3; p<0.01).

(q) Graph on the reduced C-FLIP mRNA expression after STS in presence of Lovastatin (Control normalised 1; control + STS 1.49±0.32; lovastatin .052±0.1; lovastatin +STS .85±0.10; n=3; p<0.01).

(r) Graphical representation of the hypothetical mitochondrial-nuclear interaction domain in which, mitochondrial proximity to the nucleus under apoptotic conditions can result in movement of TSPO, cholesterol, ROS, and oxysterols from the mitochondrial outer membrane to the nucleus, as well as conversion of nuclear membrane cholesterol to oxidative derivatives. Cholesterol-binding, stress response protein TSPO mediates this interaction and hence the mitochondrial-nuclear retrograde communication.

Figure 1

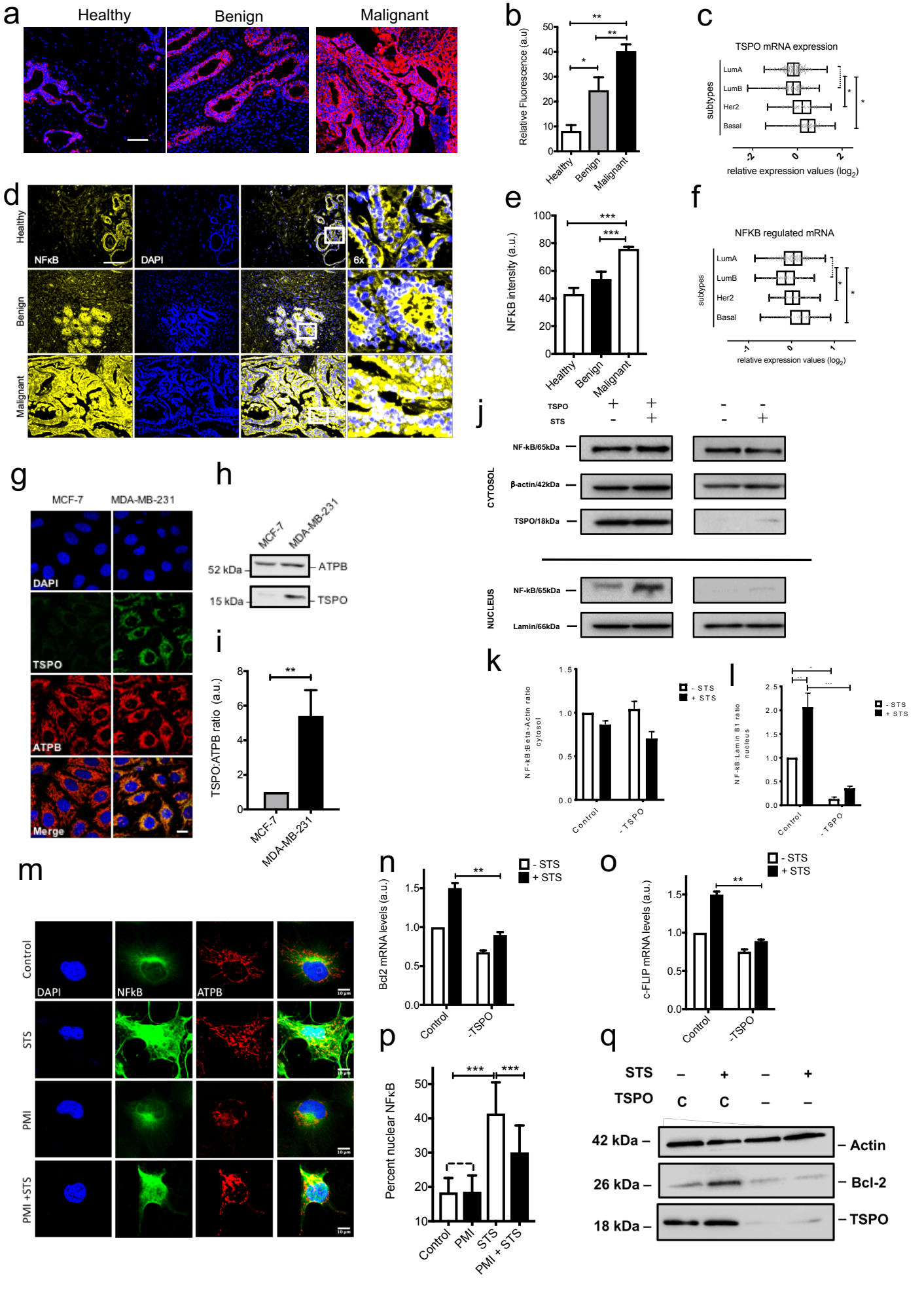
a
Healthy
Benign
Malignant
b
Relative Fluorescence (a.u)
Healthy
Benign
Malignant
c
TSPO mRNA expression
subtypes
LumA
LumB
Her2
Basal
relative expression values (log2)
d
Healthy
Benign
Malignant
NFκB
DAPI
6x
e
NFkB intensity (a.u.)
Healthy
Benign
Malignant
f
NFKB regulated mRNA
subtypes
LumA
LumB
Her2
Basal
relative expression values (log2)
g
MCF-7
MDA-MB-231
DAPI
TSPO
ATPB
Merge
h
MCF-7
MDA-MB-231
52 kDa
ATPB
15 kDa
TSPO
i
TSPO:ATPB ratio (a.u.)
MCF-7
MDA-MB-231
j
TSPO
STS
NF-kB/65kDa
β-actin/42kDa
TSPO/18kDa
CYTOSOL
NF-kB/65kDa
Lamin/66kDa
NUCLEUS
k
N F-kB:Beta-Actin ratio cytosol
- STS
+ STS
Control
-TSPO
l
N F-kB:Lamin B1 ratio nucleus
- STS
+ STS
Control
-TSPO
m
Control
STS
PMI
PMI +STS
DAPI
NFkB
ATPB
n
Bcl2 mRNA levels (a.u.)
- STS
+ STS
Control
-TSPO
o
c-FLIP mRNA levels (a.u.)
- STS
+ STS
Control
-TSPO
p
Percent nuclear NFκB
Control
PMI
STS
PMI + STS
q
STS
TSPO
42 kDa
Actin
26 kDa
Bcl-2
18 kDa
TSPO

Figure 2

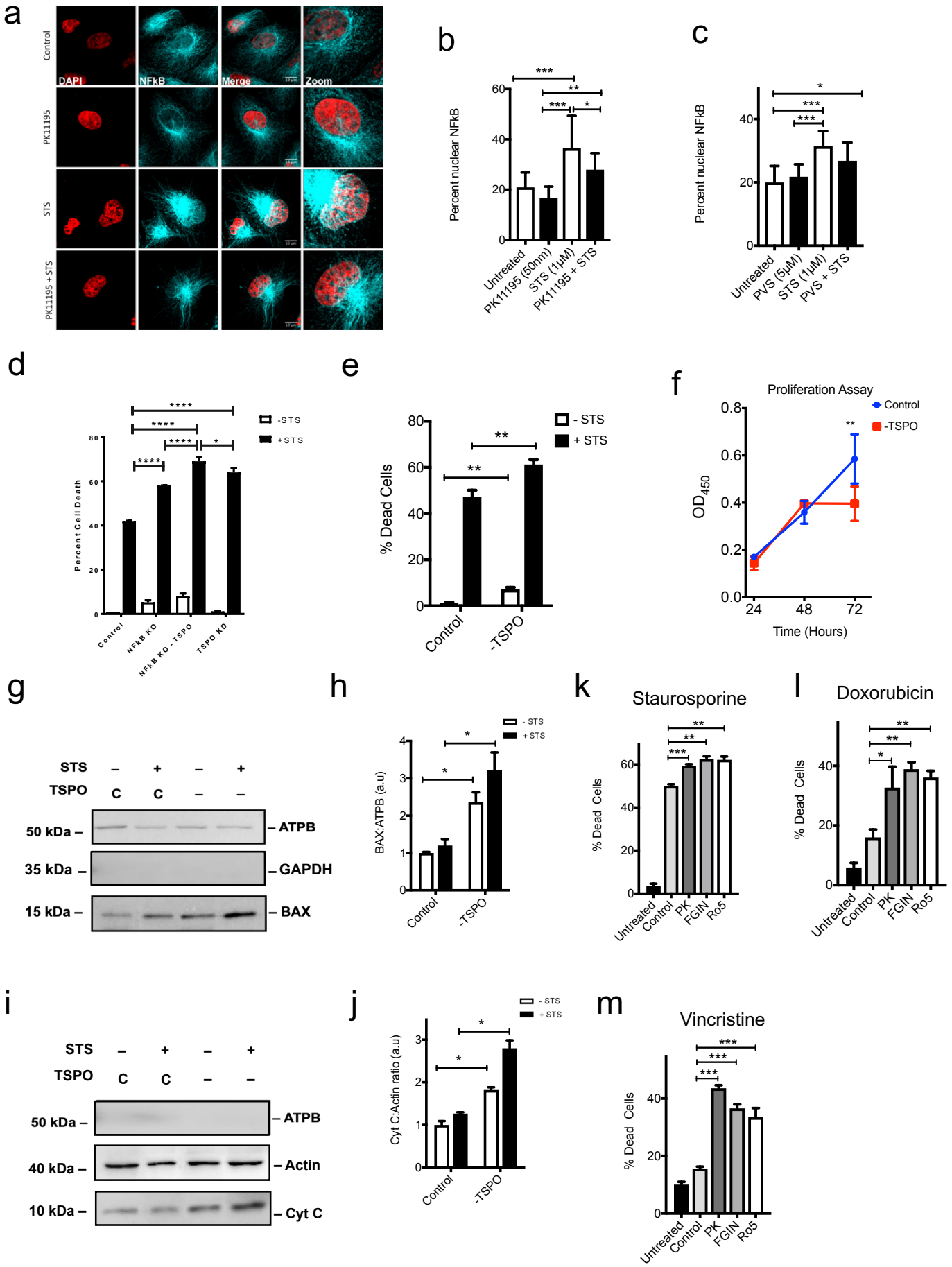
a
Control
PK11195
STS
PK11195 + STS
DAPI
NFkB
Merge
Zoom
b
Percent nuclear NFkB
Untreated
PK11195 (50nm)
STS (1μM)
PK11195 + STS
c
Percent nuclear NFkB
Untreated
PVS (5μM)
STS (1μM)
PVS + STS
d
Percent Cell Death
-STS
+STS
Control
NFkB KO
NFkB KO - TSPO
TSPO KD
e
% Dead Cells
- STS
+ STS
Control
-TSPO
f
Proliferation Assay
Control
-TSPO
OD450
Time (Hours)
g
STS
TSPO
50 kDa
35 kDa
15 kDa
ATPB
GAPDH
BAX
h
BAX:ATPB (a.u)
- STS
+ STS
Control
-TSPO
k
Staurosporine
% Dead Cells
Untreated
Control
PK
FGIN
Ro5
l
Doxorubicin
% Dead Cells
Untreated
Control
PK
FGIN
Ro5
i
STS
TSPO
50 kDa
40 kDa
10 kDa
ATPB
Actin
Cyt C
j
Cyt C:Actin ratio (a.u)
- STS
+ STS
Control
-TSPO
m
Vincristine
% Dead Cells
Untreated
Control
PK
FGIN
Ro5

Figure 3

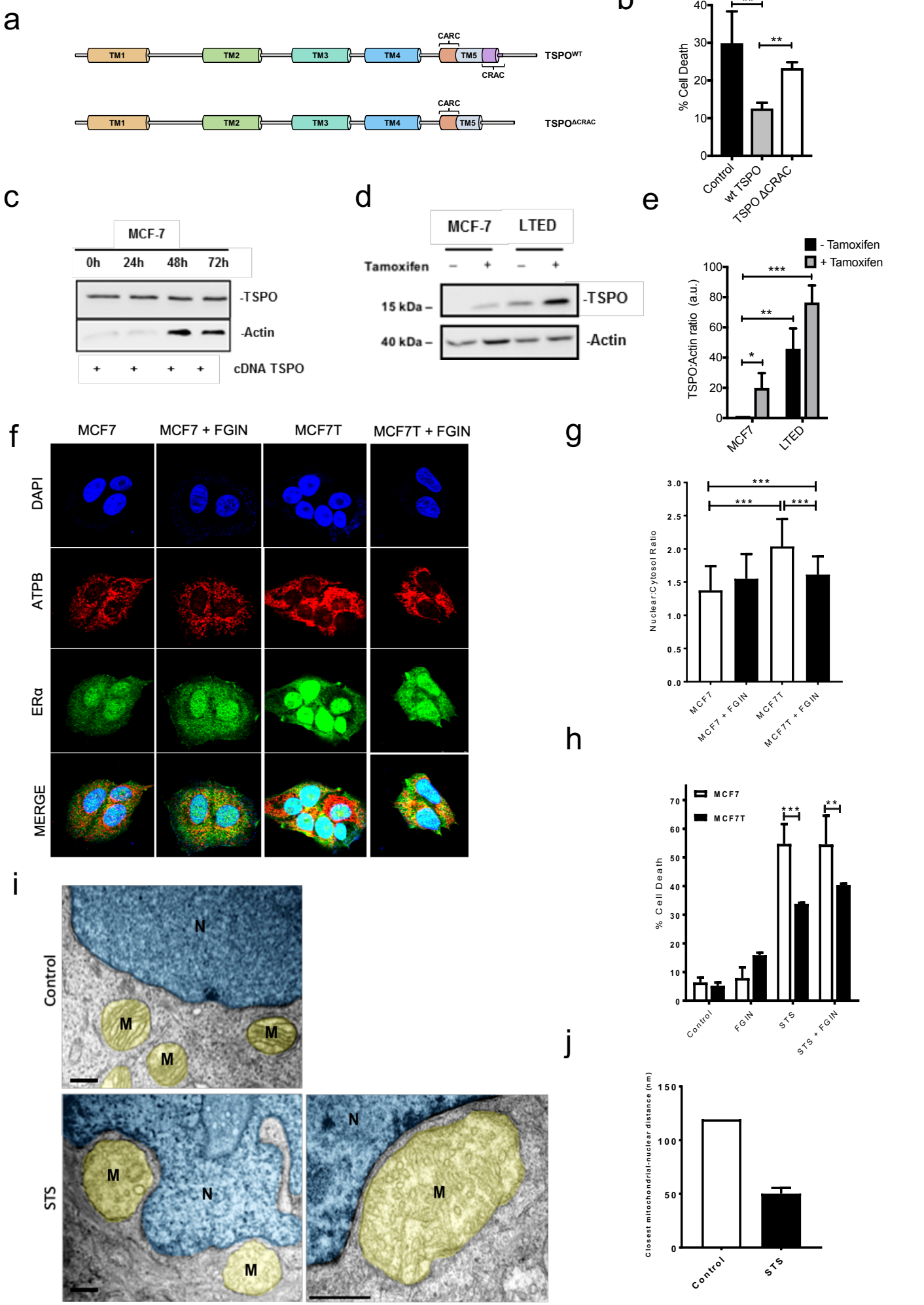
a
TM1
TM2
TM3
TM4
TM5
CARC
CRAC
TSPOWT
TSPOΔCRAC
b
% Cell Death
Control
wt TSPO
TSPO ΔCRAC
c
MCF-7
0h
24h
48h
72h
-TSPO
-Actin
cDNA TSPO
d
MCF-7
LTED
Tamoxifen
15 kDa –
40 kDa –
-TSPO
-Actin
e
- Tamoxifen
+ Tamoxifen
TSPO/Actin ratio (a.u.)
MCF7
LTED
f
MCF7
MCF7 + FGIN
MCF7T
MCF7T + FGIN
DAPI
ATPB
ERα
MERGE
g
Nuclear:Cytosol Ratio
h
MCF7
MCF7T
% Cell Death
Control
FGIN
STS
STS + FGIN
i
Control
STS
N
M
j
Closest mitochondrial-nuclear distance (nm)
Control
STS

Figure 4

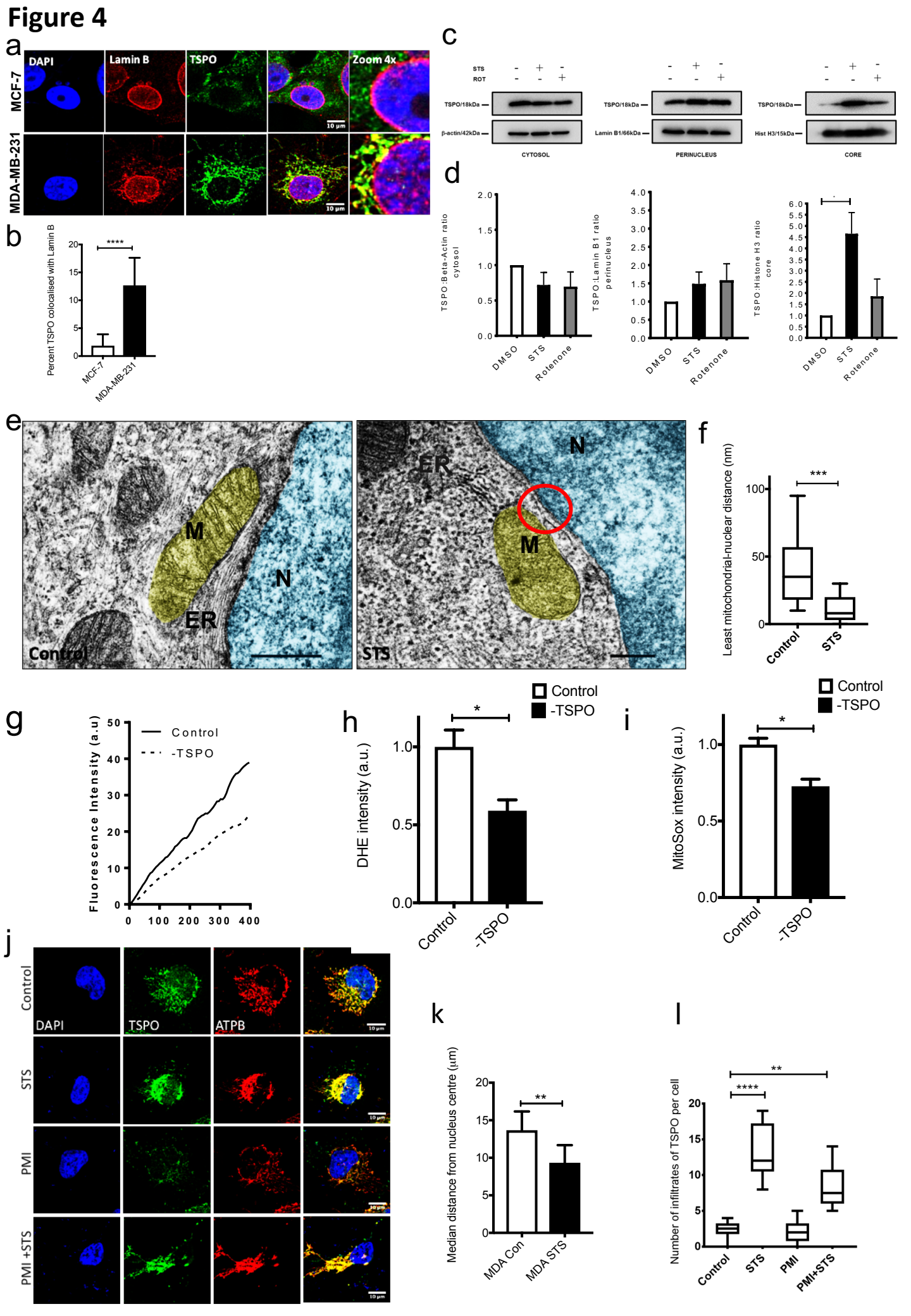
a
DAPI
Lamin B
TSPO
Zoom 4x
MCF-7
MDA-MB-231
10 µm
b
Percent TSPO colocalised with Lamin B
****
MCF-7
MDA-MB-231
c
STS
ROT
TSPO/18kDa
β-actin/42kDa
Lamin B1/66kDa
Hist H3/15kDa
CYTOSOL
PERINUCLEUS
CORE
d
TSPO:Beta-Actin ratio cytosol
TSPO:Lamin B1 ratio perinucleus
TSPO:Histone H3 ratio core
DMSO
STS
Rotenone
e
M
N
ER
Control
STS
f
Least mitochondrial-nuclear distance (nm)
***
Control
STS
g
Fluorescence Intensity (a.u)
Control
-TSPO
h
DHE intensity (a.u.)
*
Control
-TSPO
i
MitoSox intensity (a.u.)
*
Control
-TSPO
j
Control
STS
PMI
PMI +STS
DAPI
TSPO
ATPB
10 µm
k
Median distance from nucleus centre (µm)
**
MDA Con
MDA STS
l
Number of infiltrates of TSPO per cell
**
****
Control
STS
PMI
PMI+STS

Figure 5

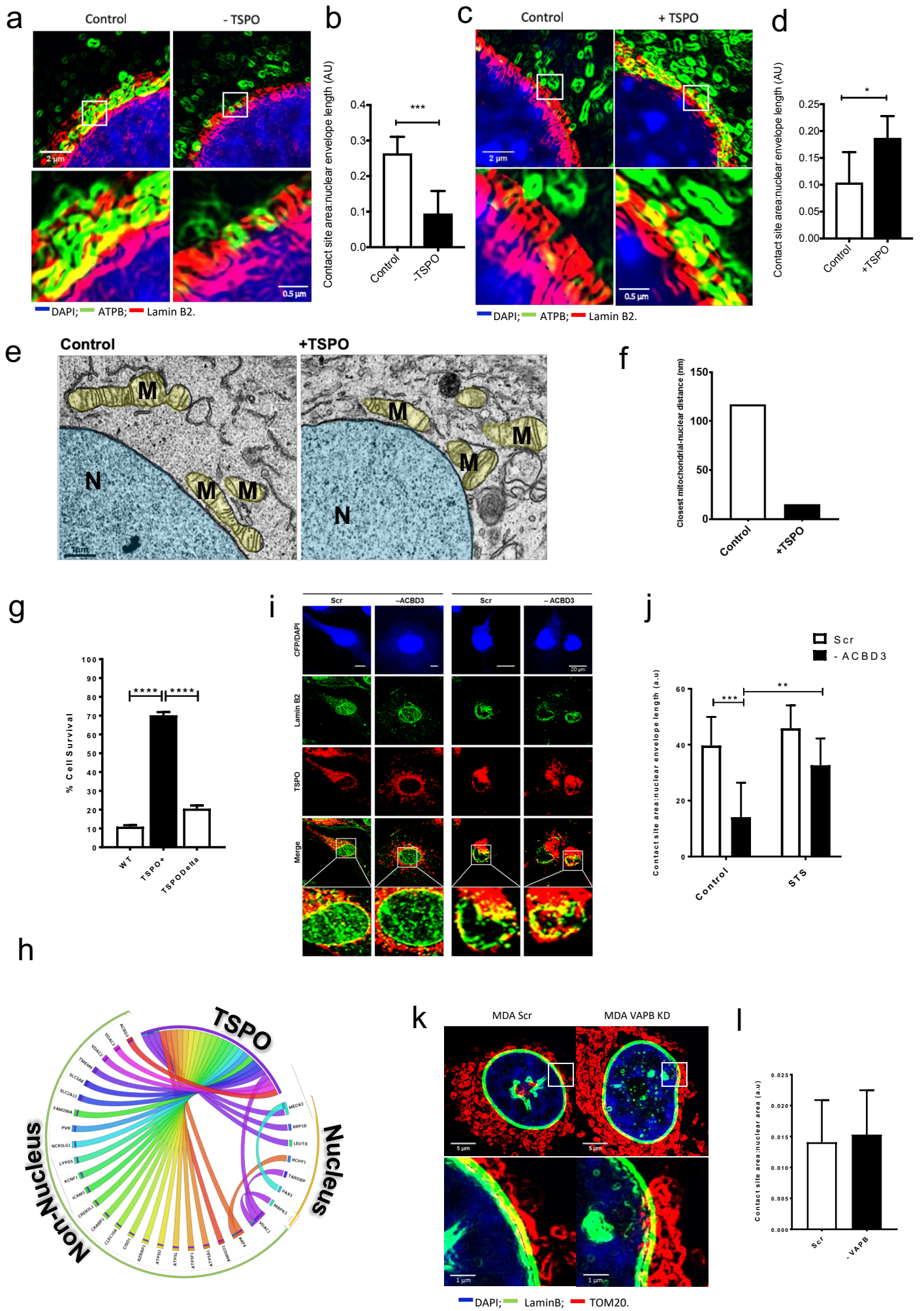
a
Control
- TSPO
2 µm
0.5 µm
DAPI; ATPB; Lamin B2.
b
Contact site area:nuclear envelope length (AU)
***
Control
-TSPO
c
Control
+ TSPO
2 µm
0.5 µm
DAPI; ATPB; Lamin B2.
d
Contact site area:nuclear envelope length (AU)
*
Control
+TSPO
e
Control
+TSPO
M
N
f
Closest mitochondrial-nuclear distance (nm)
Control
+TSPO
g
% Cell Survival
****
****
WT
TSPO+
TSPODelta
i
Scr
–ACBD3
Scr
– ACBD3
CFP/DAPI
Lamin B2
TSPO
Merge
20 µm
j
Scr
- ACBD3
Contact site area:nuclear envelope length (a.u)
***
**
Control
STS
h
TSPO
Nucleus
Non-Nucleus
k
MDA Scr
MDA VAPB KD
5 µm
1 µm
DAPI; LaminB; TOM20.
l
Contact site area:nuclear area (a.u)
Scr
- VAPB

Figure 6

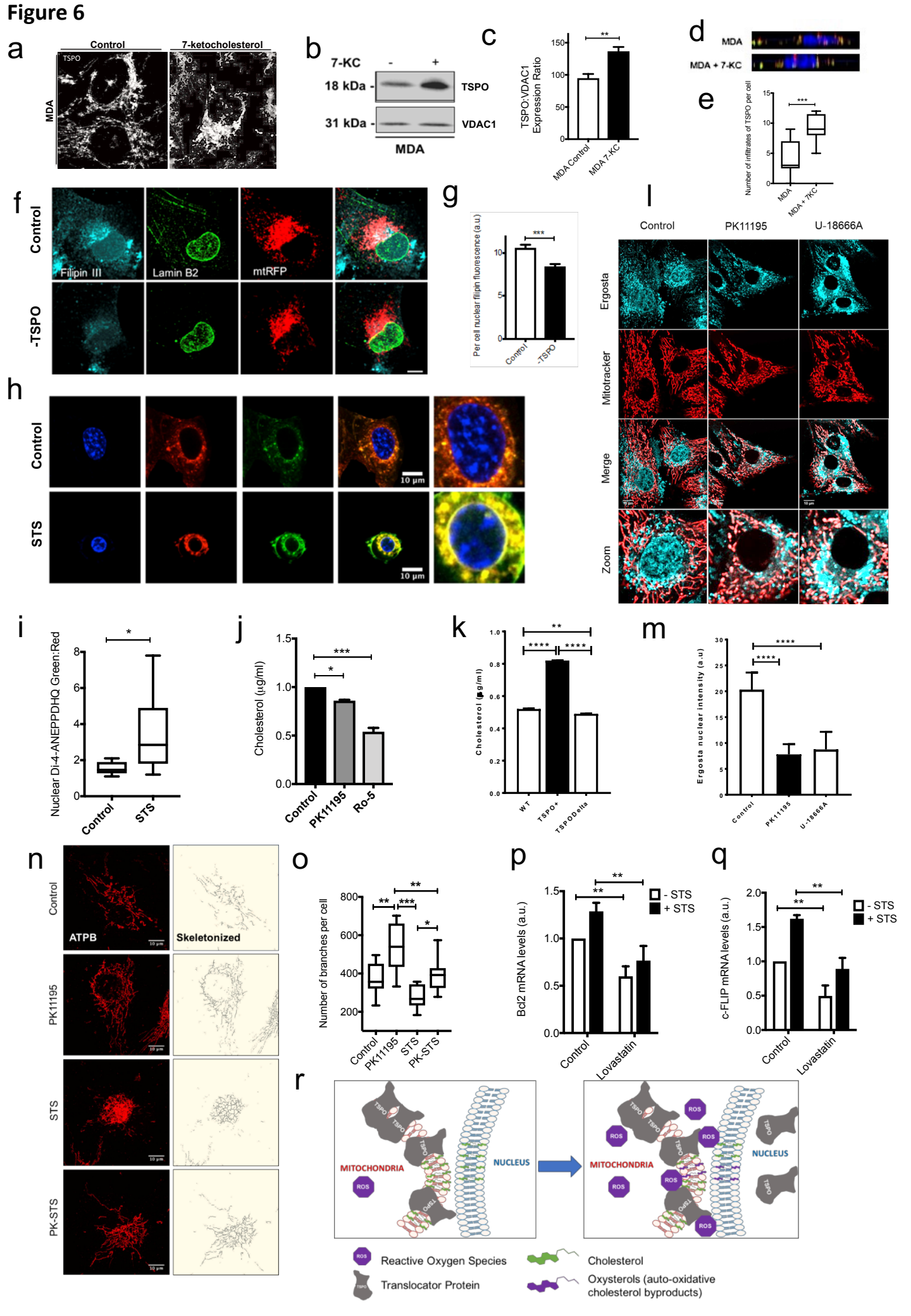
a
Control
7-ketocholesterol
TSPO
MDA
b
7-KC
18 kDa
31 kDa
TSPO
VDAC1
MDA
c
TSPO:VDAC1 Expression Ratio
MDA Control
MDA 7-KC
d
MDA
MDA + 7-KC
e
Number of infiltrates of TSPO per cell
MDA
MDA + 7KC
f
Control
-TSPO
Filipin III
Lamin B2
mtRFP
g
Per cell nuclear filipin fluorescence (a.u.)
Control
-TSPO
l
Control
PK11195
U-18666A
Ergosta
Mitotracker
Merge
Zoom
h
Control
STS
10 µm
i
Nuclear Di-4-ANEPPDHQ Green:Red
Control
STS
j
Cholesterol (µg/ml)
Control
PK11195
Ro-5
k
Cholesterol (µg/ml)
WT
TSPO+
TSPODelta
m
Ergosta nuclear intensity (a.u.)
Control
PK11195
U-18666A
n
Control
PK11195
STS
PK-STS
ATPB
Skeletonized
o
Number of branches per cell
Control
PK11195
STS
PK-STS
p
Bcl2 mRNA levels (a.u.)
- STS
+ STS
Control
Lovastatin
q
c-FLIP mRNA levels (a.u.)
- STS
+ STS
Control
Lovastatin
r
MITOCHONDRIA
NUCLEUS
ROS
TSPO
Reactive Oxygen Species
Translocator Protein
Cholesterol
Oxysterols (auto-oxidative cholesterol byproducts)